Microstructure measurements along a quasi-meridional transect in the northeastern Atlantic Ocean

E. Jurado,[1] H. J. van der Woerd,[2] and H. A. Dijkstra[1]

[1]   This study presents vertical profiles of turbulence parameters obtained in the upper 100 m of the northeastern Atlantic Ocean along a transect from tropical permanently stratified waters to subpolar seasonally stratified waters in July–August 2009. The focus is to fully characterize the vertical mixing along this transect for further studies related to phytoplankton and nutrient distributions. Derived values of temperature eddy diffusivity K_T, of temperature variance dissipation rate χ_T, and of turbulent kinetic energy dissipation rate ε indicate a northward increase of turbulent mixing below the mixed layer. In the northern stations where the wind stress is sufficiently high, the vertical distributions of ε in the mixed layer follow the wind stress scaling. The related low wind-scaling factors, and the low values of ε encountered at this cruise, are in agreement with a strongly stratified upper water column at midday in summer.

Citation: Jurado, E., H. J. van der Woerd, and H. A. Dijkstra (2012), Microstructure measurements along a quasi-meridional transect in the northeastern Atlantic Ocean, *J. Geophys. Res.*, *117*, C04016, doi:10.1029/2011JC007137.

1.   Introduction

[2]   Observations as well as results from climate models indicate that stratification patterns in the ocean may change due to global warming [*Sarmiento et al.*, 1998; *Levitus et al.*, 2000; *Toggweiler and Russell*, 2008]. Changes in stratification patterns may have major effects on the production and species composition of phytoplankton mainly due to changes in turbulent vertical fluxes of nutrients [*Behrenfeld et al.*, 2006; *Huisman et al.*, 2006; *Omta et al.*, 2007]. This will subsequently impact grazing, virally induced mortality and sedimentation rates, with cascading effects on ecosystem functioning and biogeochemical fluxes [*Kiorboe*, 1993; *Mann and Lazier*, 2006]. Little is known, however, of the exact implications of stratification for these fundamental processes.

[3]   The turbulence at the smallest scales, i.e., in the energy dissipation range, is a central issue when assessing the effects of the changes in stratification on phytoplankton [*Fasham*, 2002]. In the upper ocean, the generally stable stratification favors the largest property gradients in the vertical direction [*Osborn and Cox*, 1972] and hence a one-dimensional vertical approach is well-justified in the determination of the turbulent mixing. The properties of the vertical mixing due to small-scale turbulence are generally measured by so-called microstructure profilers. These are low-inertia free-falling instruments which measure the vertical temperature and/or the shear velocity distribution with a very high spatial resolution [*Gregg and Cox*, 1971]. Key derived turbulence quantities are the temperature eddy diffusivity K_T, computed from the temperature variance dissipation rate χ_T, and the turbulent kinetic energy (TKE) dissipation rate ε; these quantities play an important role in phytoplankton dynamics [*Peters and Marrasé*, 2000; *Huisman et al.*, 2006].

[4]   The majority of the reported microprofiler surveys in the open ocean have been carried out in the Pacific [*Osborn and Cox*, 1972; *Ozmidov*, 1973; *Gregg et al.*, 1985; *Lombardo and Gregg*, 1989; *Moum*, 1996; *Sharples et al.*, 2001; *Soloviev and Lukas*, 2003], while there are relatively few surveys of the Atlantic Ocean [*Shay and Gregg*, 1986; *Ruddick et al.*, 1997; *Lozovatsky et al.*, 2005]. Apart from early results obtained during cruises by the Russian Academy of Sciences in the Pacific [*Ozmidov*, 1973], and a longitudinal transect in the North Atlantic near 52°N [*Lozovatsky et al.*, 2005], most studies have been performed in localized regions of the open ocean or in short cruises covering no more than a few latitudinal degrees. The results indicate an upper ocean with large eddy diffusivities, highly patchy and variable, and a relatively quiescent interior deep ocean. Measured values of K_T range from 10^{-2} m^2 s^{-1} in the mixed layer to 10^{-5} m^2 s^{-1} in the deep ocean away from boundaries. Values of ε are more uniform in depth and generally range from 10^{-8} m^2 s^{-3} to 10^{-6} m^2 s^{-3}. The vertical structures of ε and χ_T in the oceanic mixed layer are strongly connected to the atmospheric forcing [*Oakey and Elliott*, 1982; *Shay and Gregg*, 1986; *Soloviev et al.*, 1988; *Lombardo and Gregg*, 1989; *Anis*, 2006]. However, empirically determined scaling factors in the open ocean are scarce.

[5]   In order to investigate how changes in the vertical stratification affect phytoplankton communities, the variation of the vertical turbulent mixing along a transect with

---

[1]Institute for Marine and Atmospheric Research Utrecht, Department of Physics and Astronomy, Utrecht University, Utrecht, Netherlands.
[2]Institute for Environmental Studies, VU University Amsterdam, Amsterdam, Netherlands.
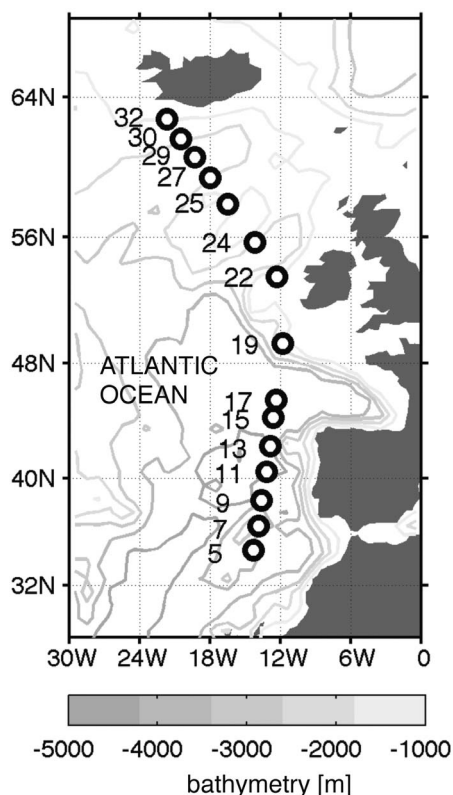
Figure 1. Map with the location of the CTD stations where the Self Contained Autonomous Microprofiler (SCAMP) measurements were carried out during the STRATIPHYT-I cruise.

variable background stratification is fundamentally important, and it should be measured with state-of-the-art methods. The STRATIPHYT-I cruise (Las Palmas, Reykjavik, 15 July to 9 August 2009) has been designed for this purpose and it has provided daytime measurements of vertical turbulent mixing, phytoplankton, and nutrients along a gradient from strong permanent stratification in the tropics to weak seasonal stratification in the subpolar region. This change in background vertical density gradients along the section provides an ideal opportunity for the comparative study of different stratification regimes.

[6] The primary objective of this study is to provide a detailed description of the vertical distribution of small-scale turbulent mixing measured in the STRATIPHYT-I cruise. In sections 2 and 3 we present the cruise data and the methodology chosen to derive the turbulence quantities K_T, χ_T, and ε. Results follow in section 4, together with the analysis of the relation between atmospheric forcing and the turbulence quantities. Further details are included in Appendix A and in the auxiliary material.[1] A summary of the results together with conclusions is provided in section 5.

2. Cruise Data

[7] The work presented here is based on temperature and conductivity miscrostructure profiles measured during the

STRATIPHYT-I cruise on board of the R/V *Pelagia* along the transect from Las Palmas de Gran Canaria (27°55′N, 15°22′W) to Reykjavik (64°6′N, 21°50′W), via Cork (51°47′N, 8°16′W). During one month (15 July to 9 August 2009), the research vessel stopped at 32 CTD stations, achieving approximately two stations per day, each station spaced apart 50 nautical miles. At 15 CTD stations, high-resolution profiles of temperature and conductivity in the upper 100 m of the ocean were measured with a microstructure profiler (section 2.1). Standard meteorological parameters were also continuously recorded during the cruise by an onboard meteorological station (section 2.2).

2.1. Microstructure Profiler Data
2.1.1. Experimental Details
[8] Temperature and conductivity were measured by a commercial microstructure profiler (Self Contained Autonomous Microprofiler, SCAMP), a battery-powered free-fall profiler designed to collect data up to 100 m depth, at a sampling rate of 100 Hz, and at a vertical fall velocity of 10 cm s^{-1} [*Stevens et al.*, 1999]. SCAMP's slow falling speed allowed to collect data at a high vertical resolution which is needed to characterize the small-scale turbulent motions. The 0.76 m long profiler (diameter 0.07 m, mass 6 kg) included two fast response thermistors, a more accurate and a stable one, a conductivity pair, and a pressure sensor. The accuracy of the fast and precision thermistors were 0.05°C and 0.02°C, respectively. The accuracy characteristics of the conductivity pair were 0.45 S/m and 0.02 S/m, and for the pressure sensor, 0.5% of the full scale range. The lowest in situ noise level of the temperature measurements was equivalent to approximately 4 10^{-9} °C^2 s^{-2} Hz^{-1}. SCAMPs have been used in a number of other field studies, most of them in coastal regions and lakes (see http://www.pme.com/HTML Docs/Scamp_Home.html for a complete record).

[9] During our cruise, the SCAMP was deployed approximately from 11 h to 15 h, with each vertical cast taking about 20 min. In order to obtain statistically robust and unbiased estimates of mean values of turbulent parameters, a large number of casts is desired. Severe weather conditions, and the impossibility to use SCAMP while the CTD was operating, were constraints to deploy the instrument, which led to a total of 148 profiles over 15 CTD stations. The geographical locations of the stations where the SCAMP was used are shown in Figure 1; details on the station properties and the number of profiles in each station are presented in Table 1. Stations with less than 3 profiles were discarded from the analysis of the station-averaged results. The largest number of profiles were obtained at the stations where the ship stayed two days (stations 17 and 30).
2.1.2. Data Processing
[10] The waves and the tension of the cable at the low-end point of the profile yield highly noisy microstructure data that need a strong refinement prior to usage. Selected starting and ending segments in the casts, which could not be recovered by any de-noising procedure, were removed from the analysis by trimming the profiles of temperature, conductivity and pressure according to the depth gradient and to the vertical gradient of the falling speed of the instrument. Sharpening and smoothing, and second-order Butterworth Brick-Wall filter, were then performed using a recursive

Table 1. Information of the CTD Stations Where the SCAMP Measurements Were Carried Out During the STRATIPHYT-I Cruise

Station	Location	Date	Profiling Start Time[a]	Number of Profiles	Traveled Distance[b] (nm)
5	34.7°N, 14.3°W	20 July 2009	11:15 h	13	250
7	36.5°N, 13.9°W	21 July 2009	11:57 h	14	350
9	38.4°N, 13.6°W	22 July 2009	11:37 h	3	450
11	40.5°N, 13.2°W	23 July 2009	11.07 h	12	550
13	42.3°N, 12.9°W	24 July 2009	11:26 h	8	650
15	44.3°N, 12.6°W	25 July 2009	11:06 h	9	750
17a	45.5°N, 12.4°W	26 July 2009	14:12 h	4	850
17b	45.5°N, 12.4°W	27 July 2009	09:04 h	6	850
19	49.3°N, 11.8°W	29 July 2009	10:52 h	14	950
22	53.6°N, 12.3°W	2 August 2009	10:02 h	5	1100
24	55.7°N, 14.2°W	3 August 2009	9:56 h	7	1200
25	58°N, 16.5°W	4 August 2009	11:06 h	1	1250
27	59.5°N, 18°W	5 August 2009	13:59 h	5	1350
29	60.7°N, 19.3°W	6 August 2009	13:23 h	7	1450
30a	61.7°N, 20.5°W	7 August 2009	11:24 h	11	1500
30b	61.7°N, 20.5°W	8 August 2009	9:03 h	14	1500
32	62.8°N, 21.7°W	9 August 2009	10:02 h	15	1600

[a]Local time of the first profile from which the profiling was done continuously, with each profile taking around 20 min.
[b]Approximate distance traveled by the ship from the beginning of the cruise.

filter technique as described by *Fozdar et al.* [1985]. Salinity was derived from the conductivity and temperature, and the density was computed using the *United Nations Educational, Scientific and Cultural Organization* (*UNESCO*) [1981] equation of state for seawater. The depth was derived from the pressure sensor by knowing the density of the surrounding water. The molecular kinematic viscosity, ν (m^2 s^{-1}), which is weakly dependent on salinity and pressure but strongly dependent on temperature, was computed from the polynomial approximation reported by the ISW-SST (1999) tool box.

[11] Values of the vertical gradient of the temperature fluctuations, $\widehat{\partial T'/\partial z}$ (the $\widehat{}$ indicating a trimmed-sharpened-smoothed-filtered quantity, T the temperature, and z the vertical coordinate), were derived from the time-based derivative of the temperature fluctuations, $\widehat{\partial T'/\partial t}$, divided by the falling speed of the microstructure profiler, $\widehat{v_{instr}}$. $\widehat{\partial T'/\partial t}$ was obtained from the de-trended (with respect to the temporal mean) time-based derivatives of the temperature. $\widehat{v_{instr}}$ was obtained from the linear least squares differentiation of the scan-based depth signal (fitting windows of 50 scans around each scan), multiplied by the sample rate of the instrument (100 Hz).

[12] The falling velocity of the SCAMP, v_{instr}, must satisfy the applicability of *Taylor*'s [1938] hypothesis of "frozen turbulence" to convert time records into vertical profiles. This assumption, common in turbulence microstructure studies, was verified by comparing the estimated turbulence velocities with the probe velocity. The turbulence velocity scales as $u \sim (\varepsilon L)^{1/3}$, where L is the root mean square of the length scale of the overturning eddies. Using the values of the centered length scale L_C [*Imberger and Boashash*, 1986], computed from the *Thorpe* [1977] displacements, L was found to have a maximum value of $\sim$10 m (Figure S1 in the auxiliary material), and the turbulent energy dissipation rate ε had a maximum value of 10^{-5} m^2 s^{-3} (section 4.1). This results in a turbulent velocity scale $u < 10^{-2}$ m s^{-1} which is considerably lower than the probe falling velocity, in the order of 0.1 m s^{-1}. Therefore, *Taylor*'s [1938]

hypothesis was used for all data segments measured by the microprofiler.

[13] In order to obtain estimates of the turbulent quantities, a further depth-binning process was performed. Depth-binning was conducted in segments of 1 m (with 700 scans in each bin approximately). The 1-m scale was chosen as a suitable trade-off between the need of high vertical resolution and the need of statistical robustness. More details of the binning procedure are presented in Appendix A.

2.1.3. Temperature, Salinity, and Buoyancy Frequency Profiles

[14] Depth-binned and station-averaged temperature, salinity and density profiles (Figure 2) show the expected variation from a warmer and saltier water column in the south to a colder and fresher water column in the north. Stations south of 40°N (similar to station 5 in Figure 2) show a decrease of salinity and temperature with depth. Taken on its own, the decrease of salinity would produce an unstable density stratified water column. However, the effect of the temperature decrease is stronger than the effect of the salinity decrease, yielding a stably stratified water column.

[15] In the stations south of 45°N, density profiles present a series of steps as a function of depth below the pynocline, commonly found in the permanently stratified water columns. The uncertainty in the station-averaged profiles is thus larger in the low-latitude stations as reflected in the 95% confidence limits in Figure 2. The scatter presented in the pynocline may be caused by the internal waves that the stratified pynocline supports.

[16] The upper nearly uniform part of the profiles in Figure 2 provides an indication for the depth of the mixed layer (MLD), ranging from 20 to 45 m. As mixed layer depth, we took the depth at which the temperature difference with respect to the surface was 0.5°C [*Levitus et al.*, 2000]. This criterion, as shown in the work of *Brainerd and Gregg* [1995], allows to have an estimate of the depth through which surface waters have been mixed in the recent past (where recent past often means within the preceding daily cycle).
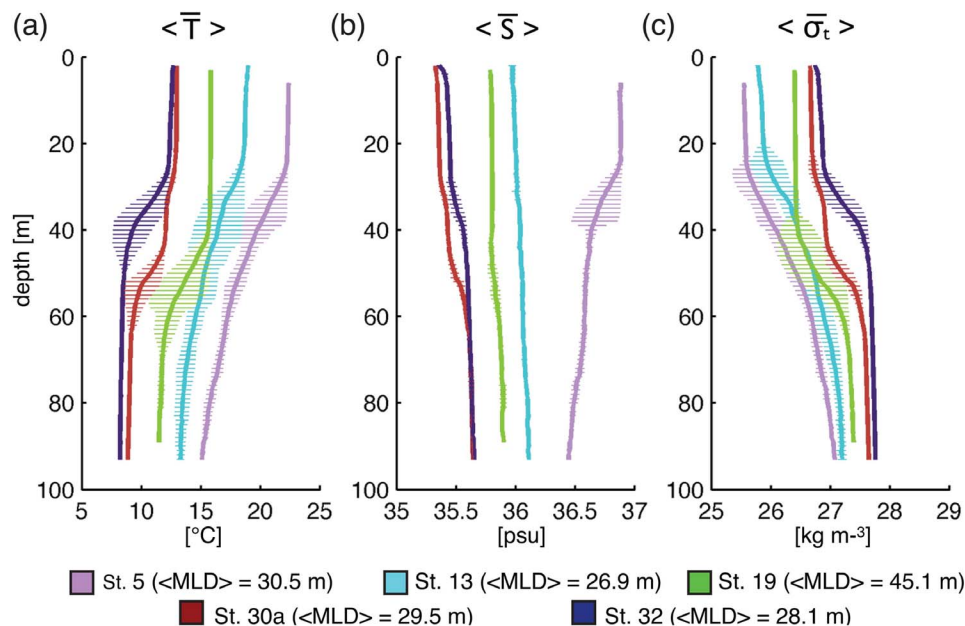
Figure 2. Profiles of (a) temperature T, (b) salinity S, and (c) sigma-t σ_t (density $\rho - 1000$) at 5 selected stations. The 95% confidence limits around the station-average are also shown. The legend shows the station number and the mixed layer depth (MLD). The overbar indicates a trimmed-smoothed-sharpened-filtered and binned quantity, and the angle brackets indicate a station-average.

[17] The strength of the background stratification in the water column was quantified with the buoyancy (Brunt-Väisälä) frequency N (rad s^{-1})

$$N = \sqrt{-\frac{g}{\rho_0}\frac{\partial \overline{\rho}}{\partial z}} \qquad (1)$$

where g (m s^{-2}) is the gravitational acceleration, $\overline{\rho}$ (kg m^{-3}) is the trimmed-smoothed-sharpened-filtered and also depth binned (hereafter referred to as TSSFB) water density, ρ_0 is a reference density, and z indicates the vertical coordinate (positive upward) in m.

[18] Figure 3 presents the buoyancy frequency along the transect, with the bins with static instabilities ($N^2 < 0$) marked in grey. The static instabilities are an important source of turbulence generation in the ocean, as they involve the release of potential energy through the descent of a plume of denser water and the ascent of a plume of lighter water. The distribution of the buoyancy frequency clearly shows the evolution from the permanently stratified waters to the seasonally stratified waters, as seen in the decrease of N just below the MLD in the high-latitude stations. The relative standard deviations due to bin-averaging, RSD_{bin}, of the values depicted in Figure 3 range between 40% and 380%, with a mean of 53%. Higher values of RSD_{bin} were
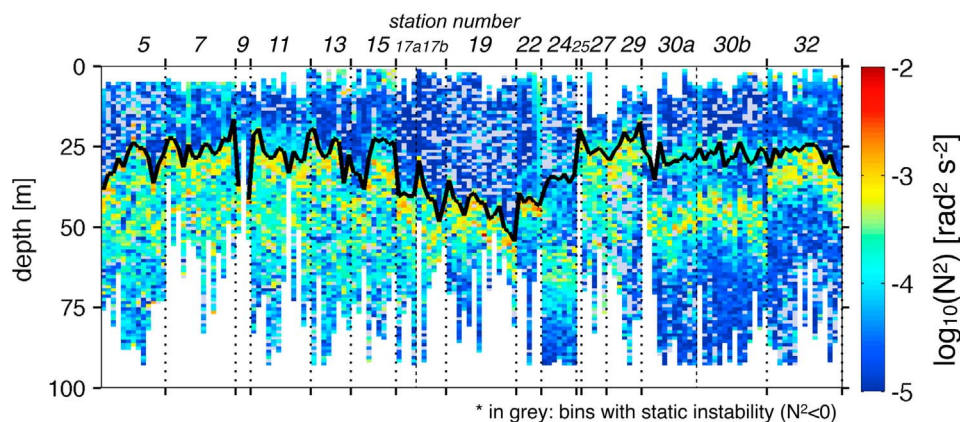

Figure 3. Depth-binned profiles of the squared buoyancy frequency N^2, derived from the SCAMP measurements along the transect. Dotted vertical lines delimit the sampling stations and the number of the corresponding station is shown at top. The mixed layer depth (MLD) for each cast is also plotted as the thick black curve.
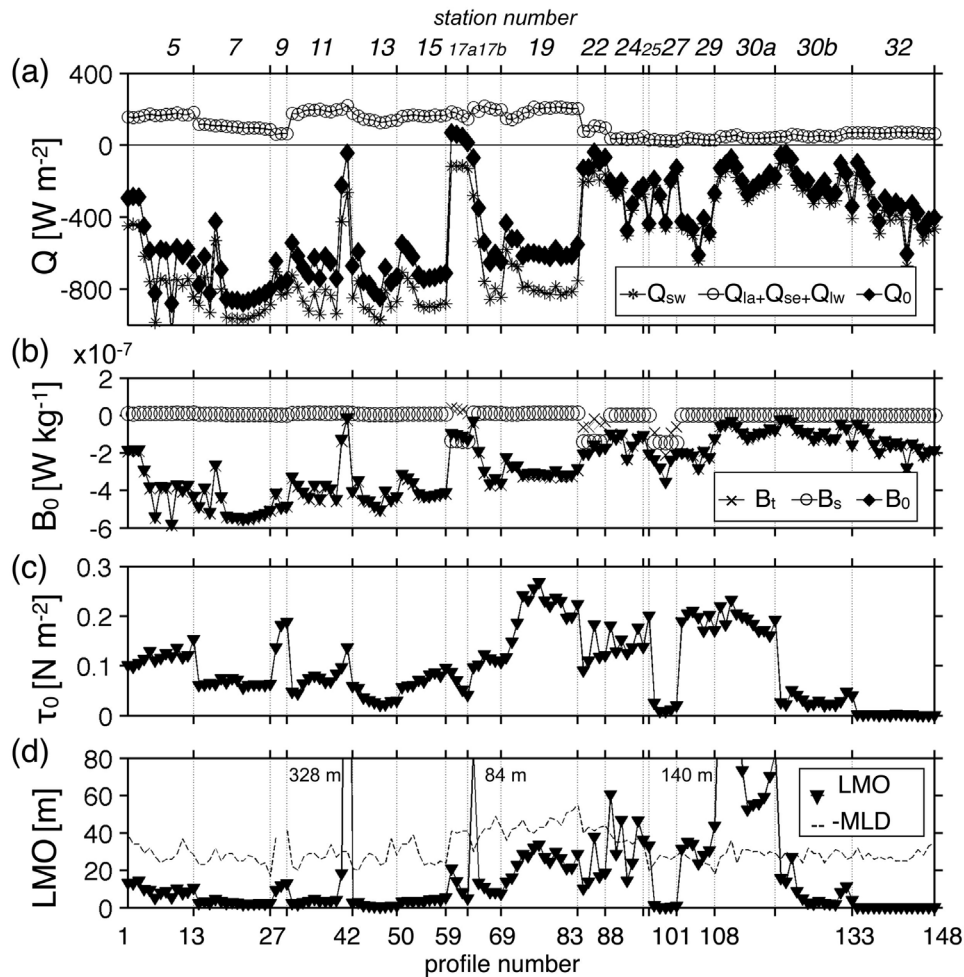
Figure 4. Meteorological data averaged over the time of each SCAMP profile: (a) net surface heat flux Q_0 and related components (latent heat flux Q_{la}, sensible heat flux Q_{se}, net long-wave heat flux Q_{lw}, short-wave radiation flux Q_{sw}); (b) net surface buoyancy flux B_0 and related components (thermal surface buoyancy flux B_t, haline surface buoyancy flux B_s); (c) surface wind stress τ_0; and (d) Monin-Obukhov length LMO, and mixed layer depth MLD. Q_0 is defined positive upward, and hence for $B_0 < 0$ the buoyancy flux is stabilizing. Each marker represents a profile, and each dotted vertical line indicates the last profile of each sampling station. The number of the corresponding station is shown at top.

located close to the surface and in the thermocline (see Appendix A for details about the computation of RSD_{bin}).

2.2. Meteorological Data

[19] The onboard meteorological station measured air temperature, humidity, wind speed and direction, downward short-wave radiation flux, and air pressure. Data was sampled every minute and stored as averages over the time of each SCAMP cast. Cloud cover and wave height were estimated from observations made every 3 hours; the rainfall rate was estimated 2 mm h^{-1} during the raining days (stations 17a, 22, and 27). Together with the sea surface temperatures and the sea surface salinity derived from the extrapolation to the surface from those measured by the microstructure profiler, the meteorological data was used to compute the net surface heat flux Q_0, the net surface buoyancy flux B_0, and the surface wind stress τ_0. These quantities allow to assess the relation between the atmospheric forcing and the upper ocean turbulence, as will be

presented in section 4.2. The calculations of Q_0 and τ_0 were performed with the Matlab Air-Sea toolbox (version 2.0, http://sea-mat.whoi.edu), which employs a simplified version of the *Fairall et al.* [1996] TOGA/COARE code. The calculation of the net surface buoyancy flux ($B_0 = B_t + B_s$) was obtained from the thermal buoyancy flux ($B_t = g\alpha Q_0/(\rho_s C_{pw})$, with α the thermal coefficient of expansion of seawater, ρ_s the water density at atmospheric pressure, C_{pw} the specific heat capacity of seawater) and from the haline buoyancy flux ($B_s = g\beta(E - P)S_0$, with β is the coefficient of haline contraction of seawater, S_0 the surface salinity, and $E - P$ the difference between the evaporation rate and the precipitation rate).

[20] During the cruise, the net surface heat flux was directed from the atmosphere to the ocean at most of the SCAMP casts (Figure 4). The related net surface buoyancy fluxes ranged from -5.8×10^{-7} to -1.2×10^{-8} W kg^{-1} (Figure 4b) and were always stabilizing the upper ocean. Note that in this paper we define the heat fluxes (and net

surface buoyancy fluxes B_0) as negative when directed downward (from the atmosphere to the ocean) and thus $B_0 < 0$ indicates a buoyancy flux stabilizing the ocean. The surface wind stress ranged from 0.0 to 0.3 N m^{-2} (Figure 4c) and was derived from wind speeds that ranged from 1.0 to 12.2 m s^{-1} at 10 m height (Figure S2 in the auxiliary material). The meteorological quantities indicate a progression from more fairly constant station-averaged wind stress and more negative surface buoyancy fluxes in the lower latitude stations, toward more extreme station-averaged wind stress and buoyancy fluxes only slightly stabilizing the upper ocean.

[21] An additional meteorological-related quantity, the Monin-Obukhov length (LMO, m), was computed for each cast of the cruise as $LMO = -u_*^3/(\kappa B_0)$, where $u_* = (\tau_0/\rho_s)^{1/2}$ (m s^{-1}) is the surface friction velocity and $\kappa = 0.4$ is the von Kármán constant. Along the transect, we find LMO > 0 (note that $B_0 < 0$), indicating that the mechanically (wind) generated turbulence is suppressed by the stable stratification. Larger values of LMO, indicating a stronger wind generated turbulence or weaker stratification, tended to occur in the high-latitude stations. LMOs were generally lower than the respective MLD, indicating that the wind-induced mixing at the time of sampling could not explain the turbulence over the total depth of the mixed layer (Figure 4d).

3. Determination of Turbulent Quantities

[22] Values of the temperature eddy diffusivity, K_T (m^2 s^{-1}), were determined from the temperature microstructure measurements using the *Osborn and Cox* [1972] model. Assumptions in the *Osborn and Cox* [1972] model include a stationary balance of the variance of temperature fluctuations, homogeneous and isotropic turbulence, dominance of the vertical heat fluxes over horizontal ones, and the omission of the divergence of the transport terms by the mean flow. K_T was computed from the temperature variance dissipation rate, χ_T (°C^2 s^{-1}), according to

$$\chi_T = 6D_T \overline{\left(\frac{\partial T'}{\partial z}\right)^2} \quad ; \quad K_T = \frac{\chi_T}{2}\left(\frac{\partial \overline{T}}{\partial z}\right)^{-2} \quad (2)$$

where D_T is the molecular diffusivity of heat ($\approx 1.4\ 10^{-7}$ m^2 s^{-1}). The determination of the vertical gradient of the TSSFB temperature, $\partial \overline{T}/\partial z$, and the determination of the TSSFB temperature fluctuations gradient, $\overline{\partial T'/\partial z}$, and the related uncertainty, are described in Appendix A. It should be noted that both K_T and χ_T, as derived from (2), are 1-m depth-binned quantities.

[23] The TKE dissipation rate, ε (m^2 s^{-3}), is usually calculated from the vertical shear velocity fluctuations of the flow. Because the profiler used in this study had no sensors of velocity microstructure, ε was estimated by fitting in each 1-m segment the theoretical *Batchelor* [1959] spectrum of the vertical gradient of the temperature fluctuations to the observed spectrum of the vertical gradient of the temperature fluctuations [*Oakey*, 1982]. We used the maximum likelihood method developed by *Ruddick et al.* [2000], which has an explicit incorporation of the instrumental noise, and allows an automated rejection of the segments that poorly fit the spectra. The spectrum of the temperature fluctuations

gradient was obtained using a fast Fourier transform with a Hamming window. The noise spectrum was modeled under the assumption that the noise is the result of white noise from the thermistor passing through the SCAMP spatial derivative channel; and other theoretical–electronic considerations are already corrected for in the host SCAMP software.

[24] In each segment, the representative ε was determined from the corresponding optimal value of the Batchelor wave number ($k_{Bsegment}$ cpm):

$$\varepsilon_{segment} = \left(2\pi k_{Bsegment}\right)^4 \nu_{segment} D_T^2 \quad (3)$$

where $\nu_{segment}$ (m^2 s^{-1}) is the arithmetic mean of the molecular kinematic viscosity in the segment. Various examples of 1-m segments that passed the rejection criteria from *Ruddick et al.* [2000] are presented in Figure S3 in the auxiliary material. A reliable estimation of $k_{Bsegment}$ was critical because of the sensitivity of $\varepsilon_{segment}$ to $k_{Bsegment}$ according to (3).

[25] The Batchelor fitting is endorsed by the pioneering studies by *Dillon and Caldwell* [1980] and *Oakey* [1982], who concluded that ε determined indirectly through Batchelor fitting agrees within a factor of 2 with the ε determined from records of velocity shear. The more recent study performed in a lake by *Kocsis et al.* [1999] leads to similar conclusions. *Nash and Moum* [2002] slightly favor the theoretical temperature spectrum proposed by *Kraichnan* [1968] over the *Batchelor* [1959] spectrum. However, the physics are clearer in Batchelor's model than in Kraichnan's semi-empirical model, and we used the former as the basis of our estimations. Besides, the fitting algorithm used in this work was developed for the Batchelor spectrum and for data of SCAMP [*Ruddick et al.*, 2000]; indeed, fitting to another spectrum would lead to an increase in uncertainty due to the lack of clear rejection criteria.

[26] The MATLAB routines used to compute these turbulent quantities were partly based on the processing software provided by PME with the SCAMP system, version 1.09 (http://www.pme.com/HTML Docs/Scamp_Home.html).

4. Results and Discussion

4.1. Derived Turbulent Quantities

[27] The temperature eddy diffusivity K_T, the temperature variance dissipation rate χ_T, and the TKE dissipation rate ε show a substantial variability, with values that are in the range of reported values in the literature (Figure 5). Over the upper 100 m, the station-averaged values of K_T ($\langle K_T \rangle = 10^{-6}$–$10^{-1}$ m^2 s^{-1} within the mixed layer, $\langle K_T \rangle = 10^{-7}$–$10^{-2}$ m^2 s^{-1} below the mixed layer) and ε ($\langle \varepsilon \rangle = 10^{-8}$–$10^{-6}$ m^2 s^{-3} within the mixed layer, $\langle \varepsilon \rangle = 5\ 10^{-9}$–$10^{-6}$ m^2 s^{-3} below the mixed layer) are low, characteristic of highly stratified water columns measured at midday and in summer. The uncertainty of the turbulent quantities, expressed by the relative standard deviation RSD_{bin} as determined in Appendix A, ranges from ~80% to 200% for K_T, from ~30 to 70% for χ_T, and from ~3% to 10% for ε. A careful validation is difficult due to the inherent variability of turbulent-related quantities and the lack of reported values in the region covered by the cruise.
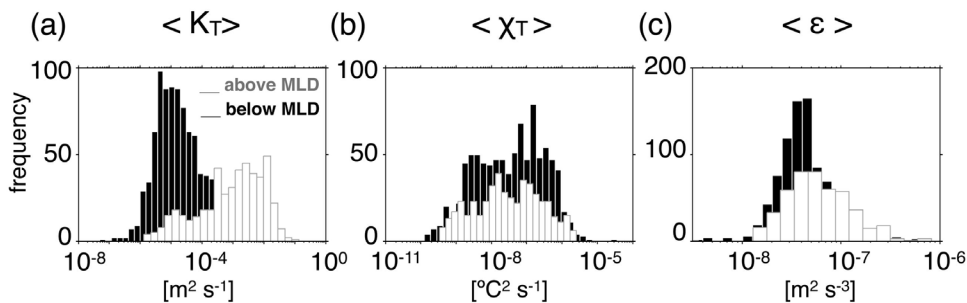
Figure 5. Histogram of the station-averaged profiles of (a) temperature eddy diffusivity K_T, (b) temperature variance dissipation rate χ_T, and (c) TKE dissipation rate ε. Bins above and below the mixed layer are distinguished. Angle brackets indicate a station-average.

[28] The values K_T (Figure 6a) peak around the middle of the mixed layer and decrease both toward the surface (where the proximity of the boundary reduces the size of the turbulent eddies) and toward the bottom of the mixed layer (where the increased water column stability reduces the turbulent mixing). Both χ_T (Figure 6b) and ε (Figure 6c) display enhanced values near the surface, which may be due to the presence of surface waves. χ_T profiles appear substantially affected by the density gradients which peak in the pynocline. The vertical distribution of ε is more uniform than that of K_T and χ_T. However, the differences of ε between one cast and another one (e.g., the one 20 min earlier) are considerable. Note that there is a large percentage (around 40%) of rejected bins for ε due to a bad fitting to a Batchelor spectrum.

[29] The inter-station variability of the turbulent quantities (Figure 7) is a distinctive feature of this study due to the large latitudinal coverage of the cruise. We observe an increase of the station- and column-averaged ε (in the mixed layer and below the mixed layer) and K_T (below the mixed layer) toward the northern stations. Within the mixed layer, K_T is more affected by the local atmospheric conditions and lacks an inter-station trend. The quantity χ_T, largely affected by thermal stratification, decreases northward. The inter-station variability may be connected to the reported northward weakening of the background stratification (Figure 3), and with the large amount of energy supplied to the ocean in the temperate regions in response to the intermittent passage of storms. Note that the inter-station tendencies are based on relatively few profiles in each station; more experimental evidence is needed to derive meaningful latitudinal trends.

4.2. Atmospheric Forcing of the Turbulent Quantities

[30] Column- and station-averaged values of temperature eddy diffusivity K_T in the mixed layer correlate positively with the wind speed (Figure 6 and Figure 7). The best linear least squares fit follows from $\langle K_T \rangle|^{-1}_{-MLD} = 0.001 \langle u_{10} \rangle - 0.003$ with a Pearson's correlation coefficient of 0.58 ($\langle \rangle$ indicates a station-average, $|^{-1}_{-MLD}$ the column-average from MLD to 1 m depth, and u_{10} is the wind speed at 10 m height). The slope of the linear regression differs significantly from zero (P-value from the linear regression t-test is 0.01, which is lower than the significance level of 0.05).

[31] Another effect of the atmospheric forcing on K_T is disclosed when analyzing its vertical distribution. K_T profiles show a sharp decrease close to the MLD when the Monin-Obukhov length is relatively large compared to the MLD (Figure 8, station 30a). Conversely, when the Monin-Obukhov length is relatively small, the profiles of K_T show a smoother decrease at the MLD (Figure 8, station 7).

[32] To investigate the relation between the TKE dissipation rate, ε, and the atmospheric forcing, we have assessed the scaling of ε with the related wind stress similarity variable, ε_{*s}. We have not assessed the scaling of ε with the related convective similarity variable because none of the measured profiles presented turbulent production dominated by convection (all the casts had downward net surface buoyancy fluxes). We have not assessed the relation of the temperature variance dissipation rate, χ_T, and the atmospheric forcing because the scaling has proven successful only when the turbulent production was dominated by convection [*Brubaker*, 1987; *Lombardo and Gregg*, 1989]. The ε_{*s} follows from

$$\varepsilon_{*s} = \frac{u_*^3}{-\kappa z} \qquad (4)$$

where z is defined positive upward, with $z = 0$ at the sea surface and $\kappa = 0.4$ is again the von Kármán constant. In conditions of dominant wind stress forcing, $\varepsilon/\varepsilon_{*s}$ was found to average around 1 in the mixed layer [*Oakey and Elliott*, 1982; *Soloviev et al.*, 1988; *Anis and Moum*, 1995], i.e., the TKE dissipation rate followed the so-called law of the wall with a proportionality constant of 1.

[33] In the STRATIPHYT-I cruise, only three stations presented mixed layers dominated by wind mixing, as determined by larger LMO compared to the MLD in all the casts of the station: station 25 (with only one cast and MLD/LMO = 0.6), station 29 ($\langle$MLD/LMO$\rangle$ = 0.8), and station 30a ($\langle$MLD/LMO$\rangle$ = 0.2). Their station-averaged ε follow the law of the wall with proportionality constants of 0.25, 0.16 and 0.21 respectively. The proportionality constants have been calculated by averaging $\langle \varepsilon/\varepsilon_{*s} \rangle$ throughout the mixed layer and avoiding the first 5 m close to the surface because of possible surface wave breaking contamination. Figure 9a depicts the profiles of scaled TKE dissipation rate for a wind-dominated mixed layer (low MLD/LMO). In this station, $\langle \varepsilon_{*s} \rangle$ normalizes $\langle \varepsilon \rangle$ to a uniform value of 0.21 in most of the mixed layer ($0.2 < -z/MLD < 0.8$). The deviation from the scaling in the first meters of water column may be related to surface wave activity [*Soloviev*
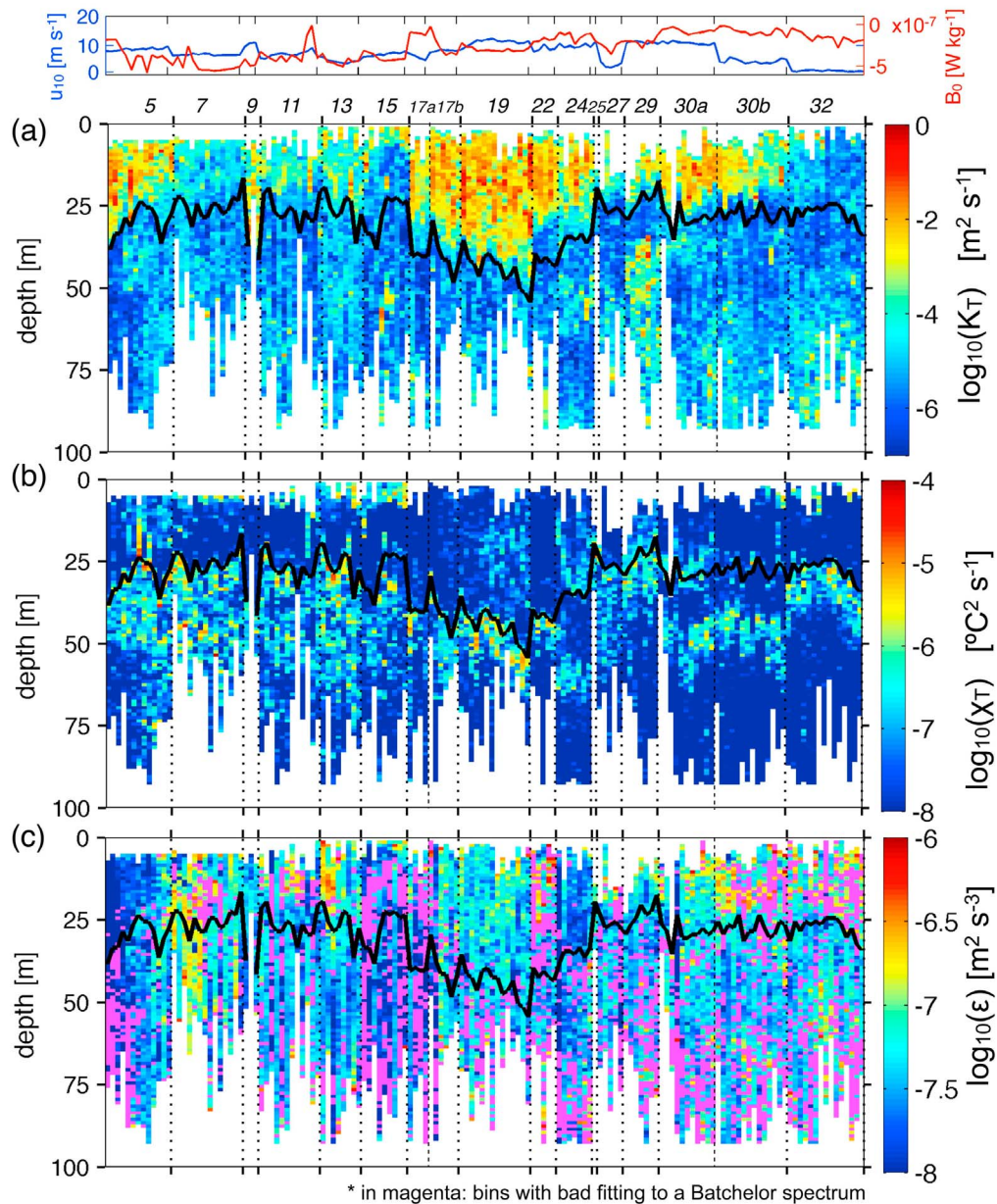
Figure 6. Depth-binned profiles of (a) temperature eddy diffusivity K_T, (b) temperature variance dissipation rate χ_T, and (c) TKE dissipation rate ε, along the transect. Dotted vertical lines delimit the sampling stations, with the corresponding number at top. The mixed layer depth (MLD) is also plotted as the thick black curve. The wind speed at 10 m height u_{10} and the net surface buoyancy flux B_0 are shown in Figure 6a.

and Lukas, 2003; *Anis*, 2006]. Figure 9b shows the scaled TKE dissipation rate for a station where the MLD/LMO ratio is relatively high. The corresponding $\langle \varepsilon \rangle$ doesn't scale with $\langle \varepsilon_{*s} \rangle$ to a uniform value, and $\langle \varepsilon \rangle$ deviates from the law-of-the-wall prediction. Note that mixed layers with relatively strong wind mixing, and thus the wind stress scaling of $\langle \varepsilon \rangle$, occurred in stations northward 45°N. It reflects the average atmospheric conditions of high-latitude regions, where wind induced mixing tends to be more important than convective mixing.

[34] The proportionality constants determined in the relation $\varepsilon/\varepsilon_{*s}$ during the STRATIPHYT-I cruise are lower than those reported at other oceanic locations. The majority of the reported empirical constants are based on measurements during nighttime [*Soloviev et al.*, 1988; *Lombardo and Gregg*, 1989; *Anis and Moum*, 1995], during winter or spring [*Lozovatsky et al.*, 2005], or in the continental shelf [*Oakey and Elliott*, 1982]. Accordingly, these studies measured higher TKE dissipation rates than those measured in STRATIPHYT-I, and explain the lower proportionality constants found here. The time shift between u_* and ε may also have contributed to a decrease in our determined empirical constants [*Lozovatsky et al.*, 2005]. Our estimated empirical constants agree with those derived from the few
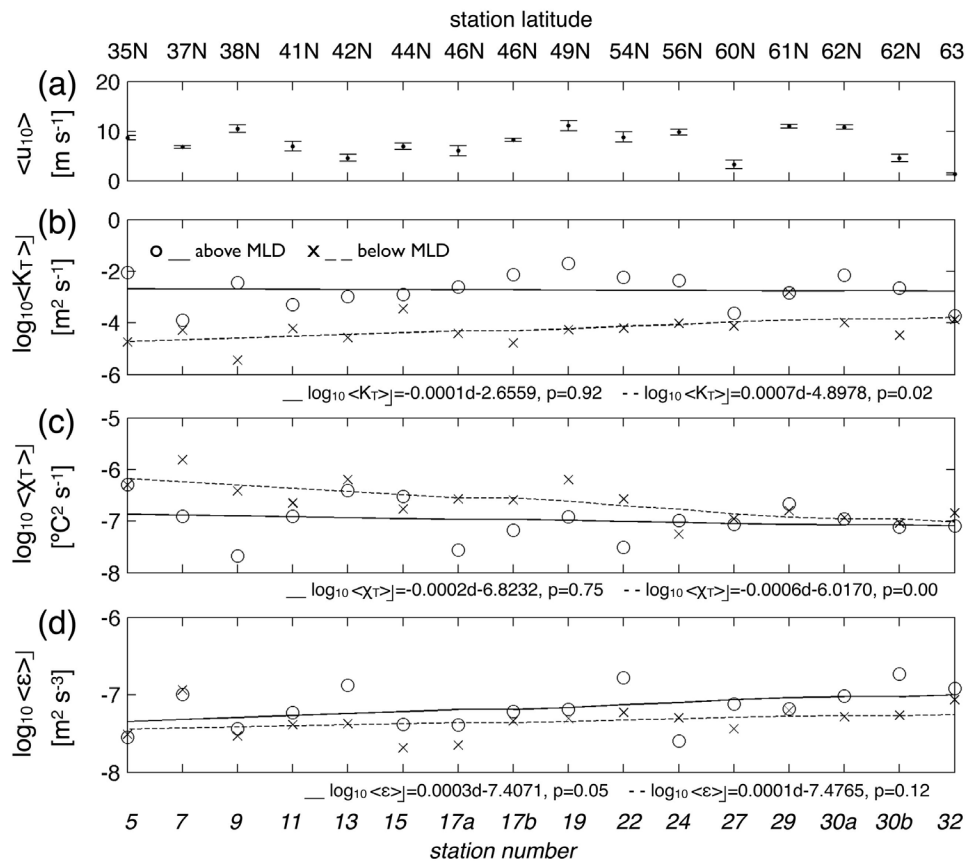
Figure 7. Station- and column-averaged turbulent quantities in the mixed layer and below the mixed layer, together with the station-averaged wind speeds. Shown are (a) wind speed at 10 m height u_{10}, (b) temperature eddy diffusivity K_T, (c) temperature variance dissipation rate χ_T, and (d) TKE dissipation rate ε. Note that station 25 is not considered because it had only one profile. The linear fitting of the column- and station-averaged turbulent quantities with the distance traveled by the ship is added (d denotes the distance in nautical miles, p denotes the P-value from the linear regression t-test). The slope of the linear regression differs significantly from 0 when p is lower than the significance level, chosen here as 0.05. The angle brackets indicate a station-average, and the notation $\rfloor$ indicates a column-average. The standard deviation of the station-averaged wind speeds is depicted in Figure 7a. The standard deviation of the values depicted in Figures 7b–7d is presented in Table S1 in the auxiliary material.

daytime summer profiles analyzed by *Anis and Moum* [1995] and *Soloviev et al.* [1988].

5. Summary and Conclusion

[35] In this study we have presented a novel data set of temperature eddy diffusivities, K_T, temperature variance dissipation rates, χ_T, and indirectly derived TKE dissipation rates, ε, in 15 ocean CTD stations from Las Palmas de Gran Canaria (27°55′N, 15°22′W) to Reykjavik (64°6′N, 21°50′W), via Cork (51°47′N, 8°16′W). The data was obtained with a commercial free-fall microstructure profiler, deployed continuously from 11 h to 15 h, during July August 2009, in the upper ~100 m of the ocean.

[36] Depth-binned and station-averaged temperature, salinity, and density profiles show the expected variation from a warmer and saltier water column in the low-latitude stations to a colder and fresher water column in the subpolar stations. The derived buoyancy frequencies, N, present also an expected change from strongly stratified water columns to weakly stratified water columns. Measured meteorological parameters indicate mixed layers dominated by wind mixing at three stations north of 45°N. Mixed layer depths (MLDs) range from 20 to 45 m, and the results presented here are representative of a tropical to subpolar Atlantic transect in the summer and during daytime.

[37] The derived temperature eddy diffusivities, K_T, display higher values in the mixed layer ($\langle K_T \rangle$: 10^{-6}– 10^{-1} m^2 s^{-1}), with both a decrease toward the surface and toward the MLD. Below the thermocline, K_T tends to be uniform, with $\langle K_T \rangle$ ranging 10^{-7} m^2 s^{-1} to 10^{-2} m^2 s^{-1}. The temperature variance dissipation rates, χ_T, present peak values in the first 10 m of the water column and at the base of the mixed layer, before reaching station-averages of 10^{-10} °C^2 s^{-1} to 10^{-7} °C^2 s^{-1} at around 100 m depth. The TKE dissipation rates, ε, present more uniform depth profiles ranging from 5 10^{-9} to 10^{-6} m^2 s^{-3}. The values are in the lower range of reported turbulence levels in the upper ocean, and are representative of strongly stratified waters at midday in summer.
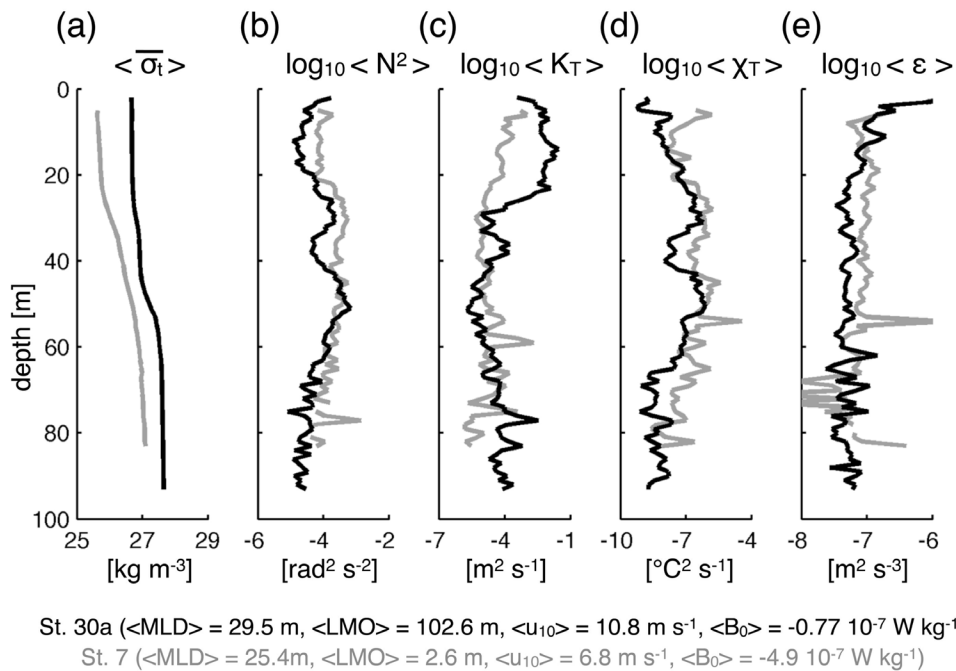
St. 30a (<MLD> = 29.5 m, <LMO> = 102.6 m, <u$_{10}$> = 10.8 m s^{-1}, <B$_0$> = -0.77 10^{-7} W kg^{-1})
St. 7 (<MLD> = 25.4m, <LMO> = 2.6 m, <u$_{10}$> = 6.8 m s^{-1}, <B$_0$> = -4.9 10^{-7} W kg^{-1})

Figure 8. Depth-binned and station-averaged profiles of turbulence quantities for a station with a small value of MLD/LMO (station 30a, black line), and for a station with a large MLD/LMO ratio (station 7, grey line). Shown are (a) sigma-t σ_t (density $\rho - 1000$), (b) squared buoyancy frequency N^2, (c) temperature eddy diffusivity K_T, (d) temperature variance dissipation rate χ_T, and (e) TKE dissipation rate ε. The legend shows the station number, and the station-averages for the mixed layer depth MLD, the Monin-Obukhov length LMO, the wind speed u_{10}, and the surface buoyancy flux B_0.

[38] Turbulent quantities, when column- and station-averaged, present distinctive inter-station gradients. Below the mixed layer, K_T has a tendency to increase toward the north and less stratified stations. χ_T, substantially affected by the density gradients, decreases toward high-latitudes, both within the mixed layer and below the mixed layer. ε increases northward, both within the mixed layer and below the mixed layer. Those latitudinal variations are in agreement with the typical increase of strong wind events at higher latitudes. Inter-station tendencies derived here are based on limited profiles; further experimental evidence and theoretical analysis is needed to be able to extract a meaningful latitudinal gradient of the turbulent quantities.

[39] Column- and station-averaged K_T in the mixed layer correlate positively with the wind speed ($\langle K_T \rangle|_{-\text{MLD}}^{-1} = 0.001 \langle u_{10} \rangle - 0.003$). In the stations with mixed layers dominated by wind mixing, as determined by larger Monin-Obukhov length compared to the MLD in all the casts of the station, TKE dissipation rates scale with the wind stress similarity variable ($\varepsilon \sim u_*^3/(-\kappa z)$) in most of the mixed layer ($0.2 < -z/\text{MLD} < 0.8$). Scaling factors range from 0.16 to 0.21, substantially lower than the commonly reported value of 1 [*Oakey and Elliott*, 1982]. The low levels of TKE dissipation rates measured in this cruise, linked to midday and summer conditions of our measurements, may explain the low scaling factors.

[40] As far as we know, the data set presented here constitutes the largest "synoptic" quasi-meridional transect of microstructure measurements in the Atlantic. The values reported here should be used with caution, they are linked to midday conditions during the northeast Atlantic summer. In

other seasons and other times of the day, the mean levels of turbulence may be higher, and also the MLD may be different. Our results hopefully will be important for providing a picture of the changes of turbulent quantities in a meridional transect with a decreasing background stratification. This data may be useful for ocean-biochemistry
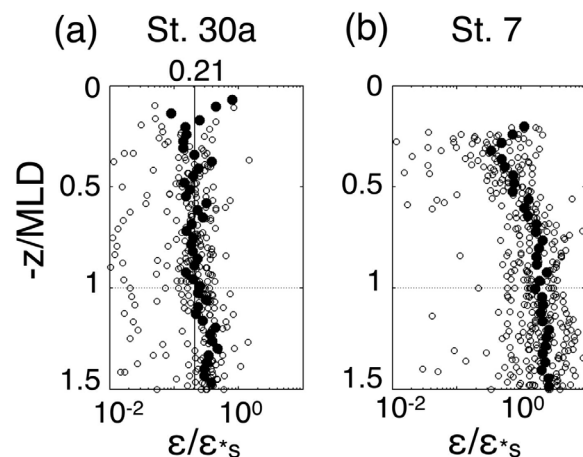

Figure 9. Scaled TKE dissipation rate with the wind stress similarity variable, $\varepsilon/\varepsilon_{*s}$, versus the scaled depth $-z/\text{MLD}$. Two characteristic stations of the cruise are shown: station 30a (Figure 9a), with $\langle \text{MLD/LMO} \rangle = 0.2$, and station 7 (Figure 9b), with $\langle \text{MLD/LMO} \rangle = 10.0$. The open circles indicate the binned individual profiles, the black filled circles indicate the binned station-averaged profiles.

models to better understand changes in nutrient and phytoplankton distributions under different stratification scenarios.

Appendix A: Averaging Procedure and Determination of Uncertainty

[41] Due to the intermittent character of turbulence, a single profile can give misleading results. For that reason, the obtained profiles of turbulent quantities along the cruise are depth-binned and station-averaged. Station-averages are obtained using the arithmetic mean. In this work we refer to the hat in $\hat{m}$ as the operation of trimming-smoothening-sharpening and filtering (also referred to as TSSF) on the quantity m; the overbar in $\overline{m}$ refers to the operation of trimming-smoothening-sharpening-filtering and also depth-binning (also referred to as TSSFB) on the quantity m. The angle brackets refer to the operation of station-averaging, and the notation $\rfloor$ refers to the operation of column-averaging.

[42] Data-binning is performed in segments of 1 m for all depths. In each segment, the TSSF data values are replaced by the segment central value, which corresponds directly to the arithmetic mean in the case of temperature T, salinity S, and density ρ. In particular, the depth-binned values of the buoyancy frequency, N, are determined by first estimating the vertical gradient of the mean (background) density, $\partial\overline{\rho}/\partial z$, obtained from the best linear least squares fit in the 1 m depth bin ($\sim$700 scans), using a 40 scans-moving average on the TSSF density versus TSSF depth. In the case of the temperature eddy diffusivity, K_T, the depth-binned value is related to $\partial\overline{T}/\partial z$, obtained from the best linear least squares fit in the 1-m bin, using a 40 scans-moving average on the TSSF and sorted temperature versus the TSSF depth. In the case of the temperature variance dissipation rate, χ_T, the segment central value is related to $\widehat{\partial T'/\partial t}$, which is obtained from the arithmetic mean of $\widehat{\partial T'/\partial t}$. Finally, the TKE dissipation rate, ε, is estimated directly for 1 m segments, and depth binning is not required.

[43] The uncertainty in a depth-binned parameter is quantified through the relative standard deviation, RSD_{bin} (%), of the bin-central value, where $RSD_{bin} = 100\ \sigma_{bin}/\mu_{bin}$ (σ_{bin} is the standard deviation and μ_{bin} the arithmetic mean in the 1-m bin of the TSSF values). The computed RSD_{bin} increases slightly with the uncertainty derived from the instrumental error. In particular, the RSD_{bin} of T, C and ρ is directly estimated as $100\ \sigma_{bin}/\mu_{bin}$. The RSD_{bin} of N is estimated from the residuals in the least squares procedure to obtain the central value of the bin. In the case of K_T, χ_T and ε, as RSD_{bin} we consider the upper limit resulting from the sum of the uncertainties of the elements in their formulae: $RSD_{bin}(K_T) = RSD_{bin}(\chi_T) + 2\ RSD_{bin}(\partial\hat{T}/\partial z)$, $RSD_{bin}(\chi_T) = 2\ RSD_{bin}(\widehat{\partial T'/\partial z}) \simeq 2\ RSD_{bin}(\partial\hat{T}/\partial z)$, $RSD_{bin}(\varepsilon) = 4\ RSD_{bin}(k_B)$. The depth-binned uncertainty of $\partial\hat{T}/\partial z$ is computed from the standard deviation and the mean of $(T_{max} - T_{min})/(z_{max} - z_{min})$ in a 40 scans-moving average. The depth-binned uncertainty of the Batchelor wave number k_B is determined from the goodness of the fit of the theoretical spectrum of the vertical gradient of the temperature fluctuations to the observed spectrum as described by *Ruddick et al.* [2000]. Additionally, the RSD_{bin}

of K_T, χ_T, and ε may increase when the uncertainties due to the assumption of a steady homogeneous isotropic turbulence and to the *Taylor* [1938] hypothesis of "frozen turbulence" are taken into account.

References

Anis, A. (2006), Similarity relationships in the unstable aquatic surface layer, *Geophys. Res. Lett.*, *19*, L19609, doi:10.1029/2006GL027268.

Anis, A., and J. N. Moum (1995), Surface wave-turbulence interactions: Scaling $\varepsilon(z)$ near the sea surface, *J. Phys. Oceanogr.*, *25*, 2025–2045.

Batchelor, G. K. (1959), Small-scale variation of convected quantities like temperature in a turbulent fluid: Part 1. General discussion and the case of small conductivity, *J. Fluid Mech.*, *5*, 113–133.

Behrenfeld, M., R. O'Malley, D. Siegel, and C. McClain (2006), Climate-driven trends in contemporary ocean productivity, *Nature*, *444*, 752–755.

Brainerd, K. E., and M. C. Gregg (1995), Surface mixed and mixing layer depths, *Deep Sea Res., Part I*, *42*(9), 1521–1543.

Brubaker, J. M. (1987), Similarity structure in the convective boundary layer of a lake, *Nature*, *330*, 742–745.

Dillon, T., and D. Caldwell (1980), The batchelor spectrum and dissipation in the upper ocean, *J. Geophys. Res.*, *85*(C4), 1910–1916.

Fairall, C. W., E. F. Bradley, D. P. Rogers, J. B. Edson, and G. S. Young (1996), Bulk parameterization of air-sea fluxes for Tropical Ocean-Global Atmosphere Coupled-Ocean Atmosphere Response Experiment, *J. Geophys. Res.*, *101*(C2), 3747–3764.

Fasham, M. (2002), *Ocean Biogeochemistry*, 297 pp., Springer, New York.

Fozdar, F., G. Parker, and J. Imberger (1985), Matching temperature and conductivity sensor response characteristics, *J. Phys. Oceanogr.*, *15*, 1557–1569.

Gregg, M. C., and C. S. Cox (1971), Measurements of the oceanic microstructure of temperature and electrical conductivity, *Deep Sea Res.*, *18*, 925–934.

Gregg, M. C., H. Peters, J. C. Wesson, N. S. Oakey, and T. J. Shay (1985), Intensive measurements of turbulence and shear in the equatorial undercurrent, *Nature*, *318*, 140–144.

Huisman, J., N. Thi, D. Karl, and B. Sommeijer (2006), Reduced mixing generates oscillations and chaos in the oceanic deep chlorophyll maximum, *Nature*, *439*(7074), 322–325.

Imberger, J., and B. Boashash (1986), Application of the Wigner-Ville distribution to temperature gradient microstructure: A new technique to study small-scale variations, *J. Phys. Oceanogr.*, *16*, 1997–2012.

Kiorboe, T. (1993), Turbulence, phytoplankton cell size and the structure of pelagic food webs, *Adv. Mar. Biol.*, *29*, 1–72.

Kocsis, O., H. Prandke, A. Stips, A. Simons, and A. Wüest (1999), Comparison of dissipation of turbulent kinetic energy determined from shear and temperature microstructure, *J. Mar. Syst.*, *21*, 67–84.

Kraichnan, R. H. (1968), Small-scale structure of a scalar field convected by turbulence, *Phys. Fluids*, *11*, 945–953.

Levitus, S., J. Antonov, T. Boyer, and C. Stephens (2000), Warming of the world ocean, *Science*, *287*, 2225–2229.

Lombardo, C. P., and M. C. Gregg (1989), Similarity Scaling of viscous and thermal dissipation in a convecting surface boundary layer, *J. Geophys. Res.*, *94*(C5), 6273–6284.

Lozovatsky, I., M. Figueroa, and E. Roget (2005), Observations and scaling of the upper mixed layer in the North Atlantic, *J. Geophys. Res.*, *110*, C05013, doi:10.1029/2004JC002708.

Mann, K., and J. Lazier (2006), *Dynamics of Marine Ecosystems: Biological-Physical Interactions in the Oceans*, 3rd ed, 489 pp, Blackwell, Malden, Mass.

Moum, J. N. (1996), Efficiency of mixing in the main thermocline, *J. Geophys. Res.*, *101*(C5), 12,057–12,069.

Nash, J. D., and J. N. Moum (2002), Microstructure estimates of turbulent salinity flux and the dissipation spectrum of salinity, *J. Phys. Oceanogr.*, *32*, 2312–2333.

Oakey, N. S. (1982), Determination of the rate of dissipation of turbulent energy from simultaneous temperature and velocity shear microstructure measurements, *J. Phys. Oceanogr.*, *12*, 256–271.

Oakey, N. S., and J. A. Elliott (1982), Dissipation within the surface mixed layer, *J. Phys. Oceanogr.*, *12*, 171–185.

Omta, A. W., B. Kooijman, and H. A. Dijkstra (2007), Influence of (sub) mesoscale eddies on the soft-tissue carbon pump, *J. Geophys. Res.*, *112*, C11009, doi:10.1029/2007JC004189.

Osborn, T. R., and C. S. Cox (1972), Oceanic fine structure, *Geophys. Fluid Dyn.*, *3*(1), 321–345.

Ozmidov, R. V. (1973), Experimental studies of small-scale ocean turbulence carried out in the P. P. Shirshov Institute of Oceanology, USSR Academy of Sciences, in *Studies of Ocean Turbulence*, pp. 3–19, Nauka, Moscow.

Peters, F., and C. Marrasé (2000), Effects of turbulence on plankton: An overview of experimental evidence and some theoretical considerations, *Mar. Ecol. Prog. Ser.*, *205*, 291–306.

Ruddick, B., D. Walsh, and N. S. Oakey (1997), Variations in apparent mixing efficiency in the North Atlantic central water, *J. Phys. Oceanogr.*, *27*, 2589–2605.

Ruddick, B., A. Anis, and K. Thompson (2000), Maximum likelihood spectral fitting: The Batchelor spectrum, *J. Atmos. Oceanic Technol.*, *17*(11), 1541–1555.

Sarmiento, J., T. Hughes, R. Stouffer, and S. Manabe (1998), Simulated response of the ocean carbon cycle to anthropogenic climate warming, *Nature*, *393*, 245–249.

Sharples, J., C. Moore, and E. Abraham (2001), Internal tide dissipation, mixing, and vertical nitrate flux at the shelf edge of NE New Zealand, *J. Geophys. Res.*, *106*(C7), 14,069–14,081.

Shay, T. J., and M. C. Gregg (1986), Convectively driven turbulent mixing in the upper ocean, *J. Phys. Oceanogr.*, *16*(11), 1777–1798.

Soloviev, A. V., and R. Lukas (2003), Observation of wave-enhanced turbulence in the near-surface layer of the ocean during TOGA COARE, *Deep Sea Res., Part I*, *50*(3), 371–395.

Soloviev, A. V., N. V. Vershinsky, and V. A. Bezverchnii (1988), Small-scale turbulence measurements in the thin surface layer of the ocean, *Deep Sea Res.*, *35*(12), 1859–1874.

Stevens, C., M. Smith, and A. Ross (1999), SCAMP: Measuring turbulence in estuaries, lakes, and coastal waters, *Water Atmos.*, *7*(2), 20–21.

Taylor, G. I. (1938), The spectrum of turbulence, *Proc. R. Soc., Ser. A*, *164*, 476–490.

Thorpe, S. (1977), Turbulence and mixing in a Scottish loch, *Philos. Trans. R. Soc. London A*, *286*, 125–181.

Toggweiler, J., and J. Russell (2008), Ocean circulation in a warming climate, *Nature*, *251*, 286–288.

United Nations Educational, Scientific and Cultural Organization (UNESCO) (1981), Tenth report of the joint panel on oceanographic tables and standards, *UNESCO Tech. Pap. Mar. Sci., 36*, 25 pp., Paris.

H. A. Dijkstra and E. Jurado, Institute for Marine and Atmospheric Research Utrecht, Department of Physics and Astronomy, Utrecht University, Princetonplein 5, NL-3584 CC Utrecht, Netherlands. (e.juradocojo@uu.nl)

H. J. van der Woerd, Institute for Environmental Studies, VU University Amsterdam, De Boelelaan 1085, NL-1081 HV Amsterdam, Netherlands.